Bulletin of the Seismological Society of America, Vol. 106, No. 5, pp. –, October 2016, doi: 10.1785/0120160073

Ⓔ

Three Ingredients for Improved Global Aftershock Forecasts: Tectonic Region, Time-Dependent Catalog Incompleteness, and Intersequence Variability

by Morgan T. Page, Nicholas van der Elst, Jeanne Hardebeck, Karen Felzer, and Andrew J. Michael

Abstract Following a large earthquake, seismic hazard can be orders of magnitude higher than the long-term average as a result of aftershock triggering. Because of this heightened hazard, emergency managers and the public demand rapid, authoritative, and reliable aftershock forecasts. In the past, U.S. Geological Survey (USGS) aftershock forecasts following large global earthquakes have been released on an *ad hoc* basis with inconsistent methods, and in some cases aftershock parameters adapted from California. To remedy this, the USGS is currently developing an automated aftershock product based on the Reasenberg and Jones (1989) method that will generate more accurate forecasts. To better capture spatial variations in aftershock productivity and decay, we estimate regional aftershock parameters for sequences within the García *et al.* (2012) tectonic regions. We find that regional variations for mean aftershock productivity reach almost a factor of 10. We also develop a method to account for the time-dependent magnitude of completeness following large events in the catalog. In addition to estimating average sequence parameters within regions, we develop an inverse method to estimate the intersequence parameter variability. This allows for a more complete quantification of the forecast uncertainties and Bayesian updating of the forecast as sequence-specific information becomes available.

Online Material: Omori parameter confidence limits, alternative Omori fits taking into account *b*-value variation, larger tectonic regions, and a longer temporal fitting window, and synthetic test results.

Introduction

Because earthquakes cluster in time and space, past earthquakes provide a great deal of information about time-dependent changes in future earthquake hazard. During an active aftershock sequence, probability gains relative to a time-independent earthquake rate model can reach several orders of magnitude (Jordan *et al.*, 2011). In some cases, aftershocks can be more damaging than mainshocks, as was the case in the 2011 M 6.3 Christchurch, New Zealand, earthquake. Furthermore, aftershocks are not always smaller than the mainshock: statistically the probability of a larger earthquake follows from the probabilities of smaller ones (Felzer *et al.*, 2004).

The statistical law that governs aftershock occurrence has been known for over 100 years (Omori, 1895). This relation, Omori's law, as modified by Utsu (1957), states that the rate of aftershocks as a function of time t from the mainshock decays as

$$\lambda(t) = K(t + c)^{-p}, \tag{1}$$

in which K, p, and c are constants. The predictability of this relation is impressive, even when extrapolated far into the future. The classic example of this predictability is the 1891 Nobi earthquake, the decay of which was studied by Omori (1895). One hundred years later, the sequence continued to follow Omori decay (Utsu *et al.*, 1995).

The U.S. Geological Survey (USGS) has issued aftershock probability reports following $M \geq 5$ earthquakes in California since the 1990s, based on the methodology of Reasenberg and Jones (1989), which combines Omori's law with Utsu scaling (the relation between the mainshock magnitude and aftershock productivity, see Utsu, 1972). In the Reasenberg and Jones (1989) formulation, the rate of aftershocks with magnitude at or above $M_{\min}$ is written as

$$\lambda(t, M_{\min}) = 10^{a+b(M_{\text{main}}-M_{\min})}(t + c)^{-p}, \tag{2}$$

in which M_{main} is the magnitude of the mainshock, and b is a constant from the Gutenberg–Richter magnitude–frequency relationship (Gutenberg and Richter, 1944). By fitting many sequences in California, Reasenberg and Jones (1989) give probability distributions for a, p, and b.

The USGS does not have a fully operational procedure for generating aftershock probability reports outside of California. However, the USGS has issued probability estimates for some global events on an *ad hoc* basis. In the cases of the 2010 M 7.0 Haiti, 2010 M 8.8 Chile, 2010 M 7.2 El Mayor–Cucapah, and 2011 M 5.8 Mineral, Virginia, earthquakes, aftershock estimates were generated using parameters fit to California data, apart from the Omori a-value, which was adjusted to match early data from the specific sequence under consideration. This approach has several drawbacks; California parameters, for example, the Omori p-value, may not be applicable elsewhere. Also, fitting the Omori a-value to the early aftershocks is only possible once those aftershocks have occurred, which introduces an undesirable delay before the first probability estimates can be issued.

In this article, we present Omori parameter estimates, using the framework of Reasenberg and Jones (1989), which can be used to generate aftershock forecasts for mainshocks occurring across the globe. We aim to improve on past work in several respects by accounting for degradation in catalog completeness following large earthquakes, by finding parameter differences between tectonic regions, and by developing a new inverse approach to solve for intersequence variability that allows us to use information from all sequences, even those sequences with few or no aftershocks.

Reasenberg and Jones (1989) with a Time-Dependent Magnitude of Completeness

Following large earthquakes, catalog completeness is worse than in quiet times; this phenomenon is known as short-term aftershock incompleteness (STAI; Kagan, 2004). Because of the changing magnitude of completeness following a large earthquake, we revise equation (2) to include a time-dependent magnitude of completeness, $M_c(t, M_{main})$, instead of a constant minimum magnitude M_{min}. The rate of aftershocks larger than $M_c(t, M_{main})$ is then given by

$$\lambda(t, M_c(t, M_{main})) = 10^{a+b(M_{main}-M_c(t,M_{main}))}(t+c)^{-p}. \quad (3)$$

We parameterize the time-varying magnitude of completeness as

$$M_c(t, M_{main}) = \max \begin{cases} \frac{M_{main}}{2} - G - \log_{10}(t) \\ M_{cat} \end{cases}, \quad (4)$$

in which M_{cat} is the known completeness of the catalog when a large earthquake has not recently occurred, and G is a constant. This function differs from previous work (Helmstetter *et al.*, 2006) in that both the amplitude of the incompleteness and the time to return to the baseline completeness M_{cat} scale with $M_{main}/2$, rather than as M_{main}. This alternative parameterization is based on an analysis of global earthquakes, as described below, and may indicate a stronger dependence on mainshock coda duration, as opposed to coda amplitude, for the large global earthquakes analyzed in this study, compared to the California dataset studied by Helmstetter *et al.* (2006). Our analysis also finds that incompleteness in the global catalog is not simply a function of earthquake rate, as suggested by Helmstetter *et al.* (2006) and assumed in more recent work by Hainzl (2016) for regional catalogs.

We estimate the parameters of the time-varying magnitude of completeness (equation 4) using a full magnitude range method (Ringdal, 1975; Ogata and Katsura, 2006; Omi *et al.*, 2014), which models the detection rate $q(m|\mu(t), \sigma)$ at magnitude m as a cumulative normal distribution:

$$q(m|\mu(t), \sigma) = \frac{1}{\sqrt{2\pi\sigma^2}} \int_{-\infty}^{m} e^{-\frac{(x-\mu(t))^2}{2\sigma^2}} dx. \quad (5)$$

The parameter σ determines the sharpness of the rollover of the detection function. In the context of a cumulative normal detection function, $\mu(t)$ can be interpreted as the level at which 50% of events are detected, and $\mu(t) + n\sigma$ gives confidence levels [68%, 95%, 99%] of event detection for $n = [1, 2, 3]$, respectively. For this study, for $M_c(t)$ we use $\mu(t) + 2\sigma$. The instrumentally recorded magnitude–frequency distribution $f(m|\mu(t), \sigma)$ is then given as the product of an exponential Gutenberg–Richter magnitude distribution (Gutenberg and Richter, 1944) and the detection function:

$$f(m|\mu(t), \sigma) \propto q(m|\mu(t), \sigma)10^{-bm}. \quad (6)$$

Omi *et al.* (2014) proposed to estimate $\mu(t)$ using a moving window on the data, with Bayesian prior and smoothing constraints to achieve a stable solution. Our approach is to assume $\mu(t) + 2\sigma$ given by equation (4) and use maximum-likelihood estimation (MLE) to determine G and σ. For simplicity, we assume $b = 1$.

Our dataset is the global National Earthquake Information Center (NEIC) catalog from 1 January 1990 to 1 January 2015 (see Data and Resources). For the purposes of this study, the mainshocks we select are $M \geq 6$ earthquakes for which there is not a larger earthquake within three fault lengths (defined for each mainshock using the Wells and Coppersmith, 1994, magnitude–length relation that averages over all focal mechanisms), for the 90 days prior to and 10 days following its occurrence. We use mainshocks down to a depth of 50 km. Aftershocks are assigned to the nearest mainshock if they occur within the larger of three fault lengths or 5 km from the mainshock. This gives a total of 2100 sequences with $M_{main} \geq 6$.

Figure 1 shows the results for all global sequences using a running-window fit for $\mu(t)$ assuming only equation (6), using separate mainshock magnitude bins and a running window of ± 0.5 log-time units. The model fit for $\mu(t)$ to the complete dataset using equations (4) and (6) is also shown.

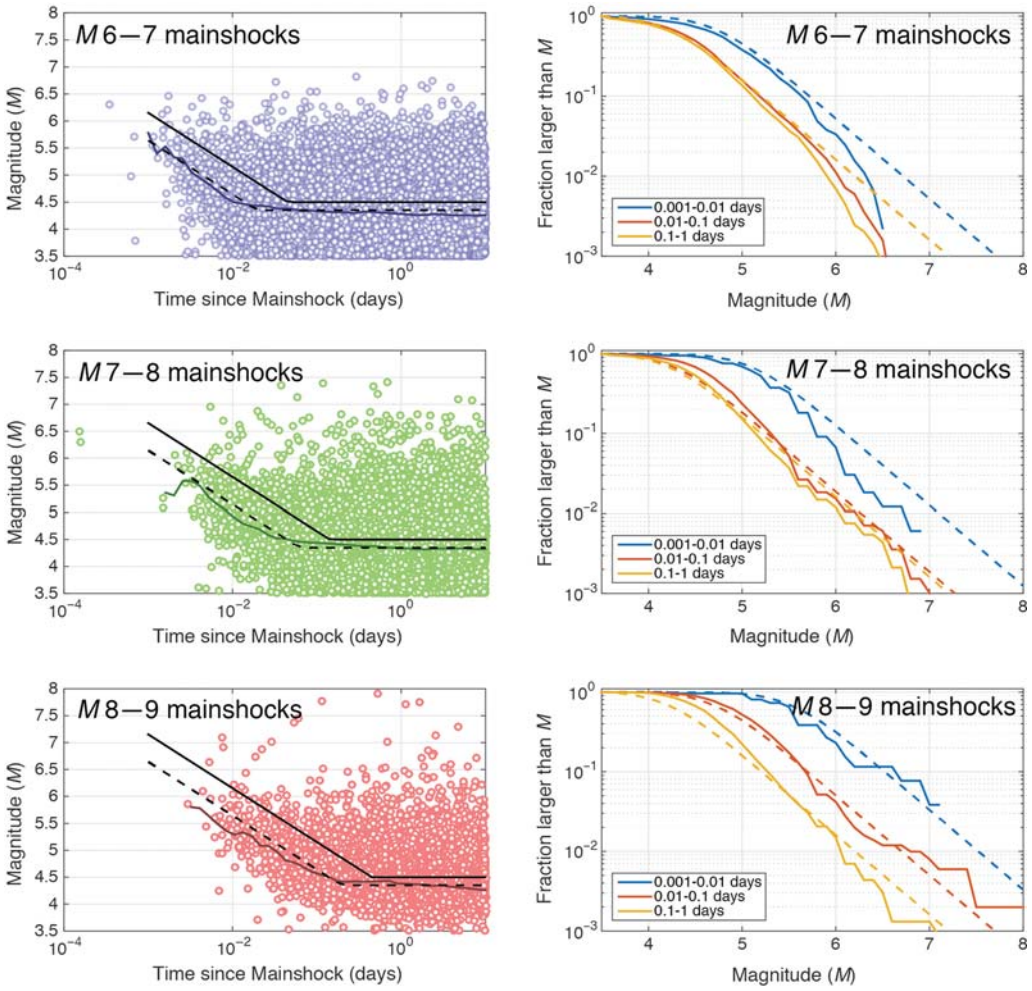

Figure 1. Time-dependent magnitude of completeness analysis for all global aftershock sequences. Irregular curves in the left panels are running fits to the 50% completeness level $\mu(t)$ for each mainshock magnitude range individually (time-window width is ± 0.5 log-time units). Dashed lines are model fits for $\mu(t)$ assuming equation (4) and fitting the entire dataset simultaneously. Solid black lines show the assumed functional dependence of $M_c(t, M_{main})$, given by equation (4) with $G = 0.25$ and $M_{cat} = 4.5$. Right panels show individual magnitude distributions for successive time ranges as a function of mainshock magnitude. Dashed lines are the model fit to the entire dataset (equations 4 and 6).

The two methods agree very closely, validating the use of equation (4). Our assumed form for $M_c(t)$, using $G = 0.25$ (found via maximum likelihood) and $M_{cat} = 4.5$ (this background completeness level fits the catalog well as a whole), is also shown.

Using equation (4) to model the time-dependent magnitude of completeness $M_c(t, M_{main})$, we use maximum likelihood to estimate the Omori parameters. Given a set of N aftershocks occurring at times t_i, the log likelihood of parameter values a and p is

$$\log L(a, p) = \sum_{i=1}^{N} \log \lambda(t_i, M_c(t_i, M_m)) - \int_{t_{beg}}^{t_{end}} \lambda(t, M_c(t, M_{main}))dt, \qquad (7)$$

in which t_{beg} and t_{end} are the beginning and end of the time period used to fit the data, respectively.

In Figure 2, we compare the performance of a forecast using the time-varying magnitude of completeness to forecasts using a constant M_c and a discretely varying M_c for the case of the 2010 M_w 8.8 Maule, Chile, earthquake. The smoothly varying M_c method shown uses the method introduced in this article, assuming $G = 0.25$ and $M_{cat} = 4.5$. A stepwise calculation of the magnitude of completeness, estimated from the data using the maximum curvature method (Wiemer and Wyss, 2000) is also shown. The a-value is computed assuming these two representations of the magnitude of completeness, and also assuming a constant magnitude of completeness of M_{cat}. To compute the a-value at a given time, all events are used that are prior to that time and above the magnitude of completeness at their time of occurrence. The exception is the stepwise magnitude of completeness, where all events within the last 4 hrs are used, except after 8 hrs, in which case all events at least 4 hrs after the mainshock are used. This method produces artificial fluctu-

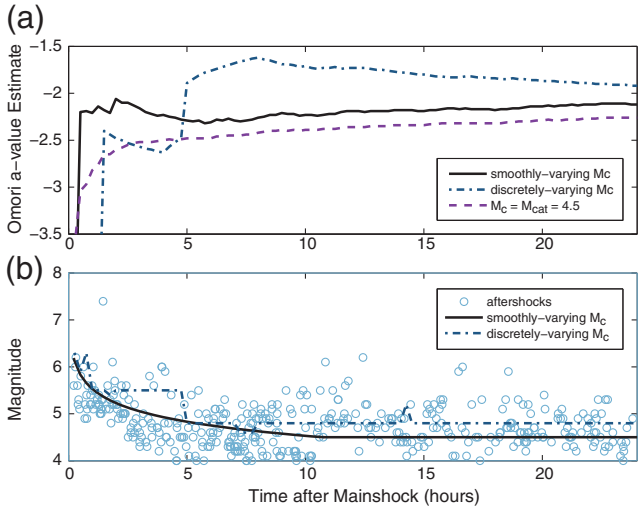

Figure 2. Maximum-likelihood fits of the (a) Omori a-value for the first day after the 2010 M_w 8.8 Maule, Chile, mainshock, computed using three different assumptions about the (b) magnitude of completeness. Assuming a constant M_c results in an unstable forecast that underestimates aftershock rates early in the sequence. The calculation with the stepwise magnitude of completeness contains abrupt changes, some aligned with the changes in the completeness, which could lead to undesirable fluctuations in the forecast as it is updated. The forecast with the smoothly varying magnitude of completeness, in contrast, produces a smooth and stable a-value over the entire first day.

ations in the forecast, which align with changes in the assumed M_c. Finally, these methods are compared with a fixed magnitude of completeness, which uses only events above the maximum magnitude of completeness in the time period used. This fixed M_c calculation underestimates the a-value because of missing early events and is not stable with time as the real completeness evolves. Incorporation of the time-varying magnitude of completeness into the likelihood calculation allows for all the data above $M_c(t)$ to be used and avoids undesirable fluctuations in the forecast.

The Reasenberg and Jones (1989) formulation assumes that aftershock productivity scales with the magnitude of the mainshock as $10^{bM_{main}}$, in which b is a constant from the Gutenberg–Richter relation (Gutenberg and Richter, 1944). Other formulations for aftershock productivity, for example, the epidemic-type aftershock sequence model (Ogata, 1988), assume productivity scales as $10^{\alpha M_{main}}$, with α not necessarily equal to b. In the case that $\alpha = b$, as we assume here, the total number of aftershocks triggered by all mainshocks within a given mainshock magnitude unit is a constant, and the Båth's law value (the magnitude difference between the mainshock and the largest aftershock, on average) is mainshock magnitude independent. The $\alpha = b$ assumption is consistent with data in California (Felzer *et al.*, 2004; Helmstetter *et al.*, 2005).

We find that the maximum-likelihood b-value (Aki, 1965) corrected for magnitude rounding (Shi and Bolt, 1982) for the NEIC catalog (1990–2015) is 1.03. This is very close to the canonical value of 1.0 (Frohlich and Davis, 1993). In the following section, we present results assuming $b = 1$ for all regions, as well as results using region-specific b-values.

Mean Omori Parameters within Tectonic Regions

To better capture spatial variations in aftershock productivity and decay, we estimate regional aftershock parameters for sequences within the García *et al.* (2012) tectonic regions, shown in Figure 3. These regions were developed for use in the USGS ShakeMap system (García *et al.*, 2012) and are modifications of the Flinn–Engdahl regionalization scheme (Flinn and Engdahl, 1965; Young *et al.*, 1996; see Data and Resources).

We select mainshocks and aftershocks using the exclusion criteria defined in the previous section. The 10-day stacked fit for the mean aftershock rate within all tectonic regions, assuming $b = 1$, is shown in Figure 4. This is a maximum-likelihood fit for all aftershocks above $M_c(t, M_{main})$, assuming $G = 0.25$ and $M_{cat} = 4.5$. For this STAI fit, we also add an inequality constraint that prevents the rate from dropping below the $M \geq 4.5$ fit for all times in the fitting interval. This prevents the STAI fit from giving a lower productivity than the $M \geq 4.5$ aftershocks imply; which would be nonsensical, because STAI can only result in fewer events in the catalog. In this way, even in the STAI fits, we use information from the catalog for events between M_{cat} and $M_c(t)$. The 95% confidence limits for the Omori parameters for each tectonic region are shown in Ⓔ Figure S1, available in the electronic supplement to this article. The inequality constraint is neglected in these confidence limits, which show the area of parameter space within three log-likelihood units of the maximum.

The exclusion criteria we use are chosen to capture as much of the aftershock triggering as possible while limiting contamination from background sources and other sequences. To test whether background events are impacting the Omori fits, we reduce the aftershock capture zone from three to two rupture lengths; this impacts the estimated p-values by less than 2% for all regions apart from ANSR-HOTSPOT, where one of the five aftershocks is lost (resulting in a 14% p-value increase—parameters in this data-poor region are quite ill-constrained). If significant background were being captured in the 10-day fits, we would expect significant p-value increases with this capture region reduction.

The mean Omori parameters from the global fit imply a median 10-day Båth's law value (the magnitude difference between the mainshock magnitude and largest aftershock magnitude, see Richter, 1958) of 1.21. In subsequent region-specific fits, we fix the Omori c-value to the c-value from this global fit ($c = 0.018$). This reduces instability for regions with a small number of sequences, especially when incorporating the STAI correction.

Fits for aftershock sequences within individual regions, assuming $b = 1$, are shown in Figure 5. Fits using region-specific b-values are shown in Ⓔ Figure S2. We show both a fit using all recorded aftershocks down to $M_{cat} = 4.5$ and a

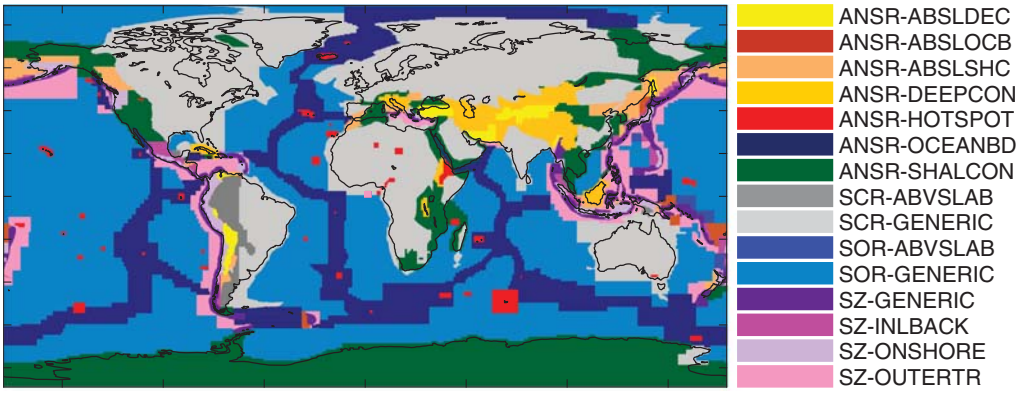

Figure 3. García *et al.* (2012) tectonic regionalization. Regions are not a function of depth. ANSR, active nonsubduction region; SCR, stable continental region; SOR, stable oceanic region; SZ, subduction zone; ABSLDEC, above-slab deep continental; ABSLOCB, above-slab oceanic boundary; DEEPCON, deep continental; OCEANBD, oceanic boundary; SHALCON, shallow continental; ABVSLAB, above-slab; INLBACK, inland/back-arc; OUTERTR, outer-trench.

fit using a STAI correction ($G = 0.25$). Estimated b-values differ from 1 most in the regions ANSR-ABSLDEC ($b = 1.20 \pm 0.03$) and SCR-GENERIC ($b = 1.25 \pm 0.08$). The SZ-GENERIC region, which dominates the global dataset, has a b-value consistent with 1.0 (1.01 ± 0.01). For the remaining results in the article, we assume $\alpha = b = 1$.

We also compute fits for the combined active nonsubduction regions (ANSRs) and subduction zone (SZ) regions, which may be preferable than the finer-scale regions that have little data. These are shown in Ⓔ Figure S3. The 100-day fits for the 13 García *et al.* (2012) regions are also shown in Ⓔ Figure S4. For longer time periods, it is preferable to extend these parameters rather than do direct fits, due to contamination from background and other sequences.

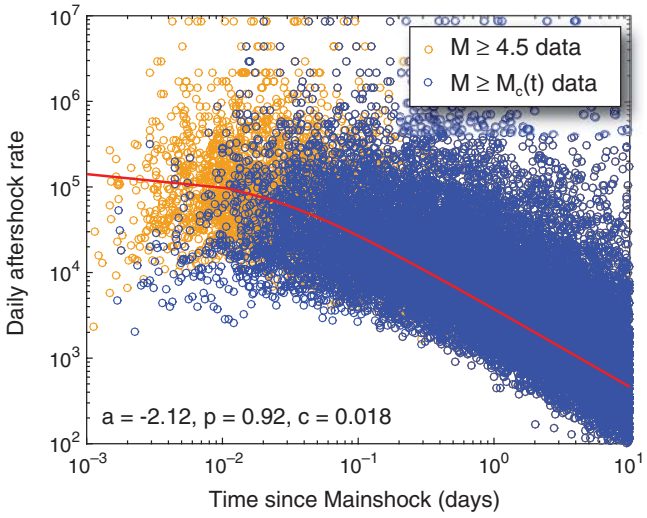

Figure 4. Maximum-likelihood fit (solid line) to the rate for all aftershocks from global $M \geq 6$ mainshocks, 1990–2015. Each data point shows the instantaneous rate for a consecutive aftershock pair.

An Inverse Method to Find Productivity Variability between Sequences

As Reasenberg and Jones (1989) note, generic aftershock parameters of the type we estimate here can be updated with Bayes' rule as data accumulate during an ongoing aftershock sequence, provided that there is a prior distribution for the generic parameters. Thus, we wish not only to estimate the mean Omori parameters, as we have done in the stack fits above, but also to estimate the intersequence variability—that is, how much the Omori parameters vary from sequence to sequence.

Investigations of the 2014 M 6.0 South Napa earthquake sequence found that updating both the Omori a- and p-values made early sequence fits unstable (Llenos, 2014). For this reason, we investigate intersequence variability of the Omori a-value, so that Bayesian updating of this parameter can be performed while the p-value is held constant. Alternatively, one could put a narrow prior on the Omori p-value, which would result in Bayesian updating of the p-value only if the data (dramatically) warranted it.

Sequence-specific fits to the productivity are difficult because half of the sequences have no aftershocks above the completeness magnitude. Reasenberg and Jones (1989) dealt with this problem by fitting only the sequences with sufficient data; however, this had the effect of overestimating the mean productivity, resulting in an informal correction whereby many researchers adjust the published value of $a = -1.67$ to $a = -1.85$ (Felzer *et al.*, 2003).

The discrete nature of the aftershocks is apparent in the sequence-specific MLE fits shown in Figure 6a. Furthermore, we expect that due to the stochasticity of aftershock occurrence, the distribution of MLE a-values, even for the sequences with many aftershocks, will have a larger spread than the true, underlying a-value distribution. To back out the underlying intersequence a-value distribution in light of these difficulties, we set up an inverse problem of the form $\mathbf{Ax} = \mathbf{d}$.

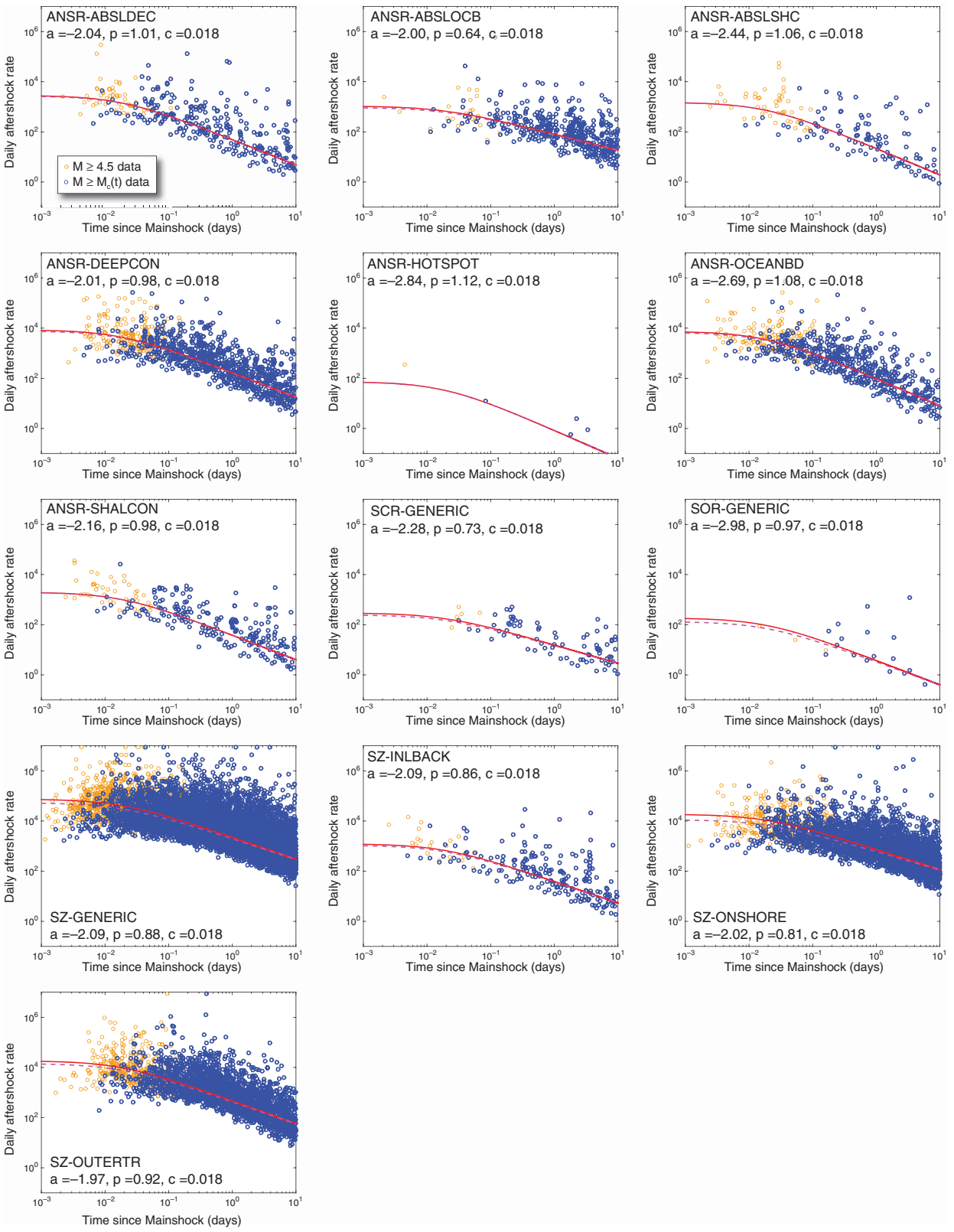

Figure 5. Stacked Omori fits for aftershock sequences within the 13 García *et al.* (2012) tectonic regions with data (Fig. 3). Dashed line, maximum-likelihood fit to the $M_{\mathrm{cat}} = 4.5$ data; solid line, maximum-likelihood fit (parameters shown in subfigure titles) for the $M \geq 4.5$ aftershock rate, using the data above $M_c(t)$. Note that the solid line should not fit the $M_{\mathrm{cat}} = 4.5$ data by eye at short times because these data are missing many $M \geq 4.5$ aftershocks. The solid-line fit does not use the $M_{\mathrm{cat}} = 4.5$ data apart from being constrained to lie at or above the dashed line for all times up to 10 days from the mainshock.

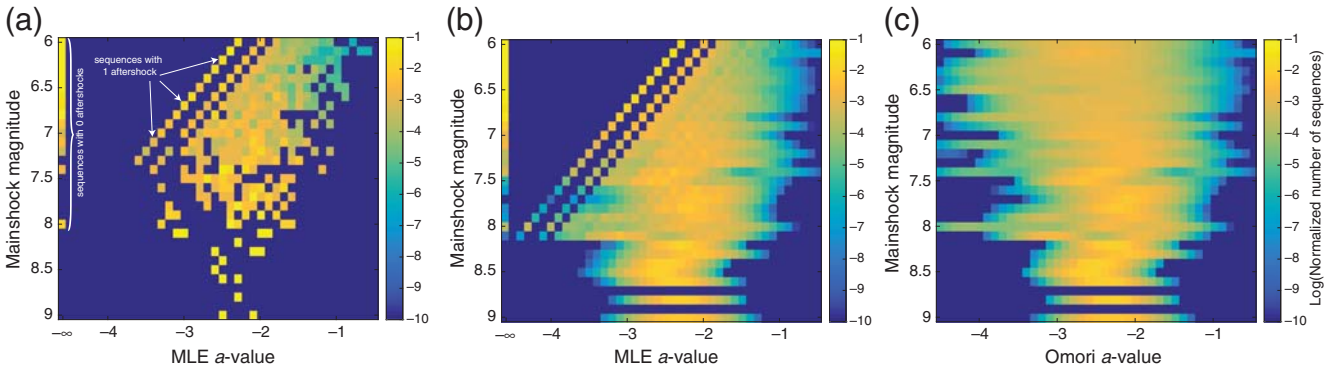

Figure 6. A visualization of the inversion (a) data vector, (b) synthetics, and (c) model (inversion result).

For each sequence, we find the MLE a-value, assuming the STAI parameter $G = 0.25$ and incorporating the inequality constraint, as was done in the stacked fits discussed above. The p-value and c-value are fixed to a sequence average for the stack, either a tectonic region or the whole globe. The data vector **d** then gives the number of sequences in each MLE a-value/mainshock magnitude bin. A visualization of the data vector for all global sequences is shown in Figure 6a.

We invert for the unknown model vector **x**, which describes the true, underlying a-value distribution that the individual sequences are sampling. The vector **x** gives the fraction of sequences in each (underlying) a-value/mainshock magnitude bin. The matrix **A** gives the mapping between true values of a and the MLE estimates of a for different mainshock magnitudes. The values of the matrix **A** are found by simulating many synthetic sequences and performing STAI fits with an inequality constraint, using the same algorithm (described in the Mean Omori Parameters within Tectonic Regions section) that is used to fit the real data. The element A_{ij} gives the fraction of sequences within the jth a-value/mainshock magnitude bin that will have an MLE estimate within the ith a-value/mainshock magnitude bin.

Elements of the model vector **x** cannot be negative, so we invert for the underlying distribution of a-values using the nonnegative least-squares algorithm (Lawson and Hanson, 1974). This algorithm gives very sparse solutions, so we additionally append Laplacian smoothing constraints. We also minimize the edges of the distribution (at $a = -4.5$ and $a = -0.5$) and constrain the mean productivity to approximately equal the productivity given by the stack of all the sequences.

We first look at the global data, inverting for the a-value distribution for each 0.1-magnitude unit mainshock magnitude bin above $M_{\text{main}} = 6$. For this dataset, we smooth only between adjacent a-value bins within a given M_{main} bin to look for systematics in productivity as a function of mainshock magnitude. The results are shown in Figure 6. Because of smoothing constraints and the stochasticity of the simulated aftershock sequences, our synthetics (given by **Ax** shown in Fig. 6b) are considerably smoother than the sparse sequence data at high mainshock magnitudes. They do reproduce the discrete a-values seen for sequences with zero or small numbers of aftershocks, as seen in the real data. Thus with the inversion method, we can use sequences without recorded aftershocks to constrain the productivity distribution.

The inversion result, or the model vector **x**, is shown in Figure 6c. This is the distribution of a-values, as a function of mainshock magnitude M_{main}, which produces the synthetics. (In these a-value distributions, the effect of the smoothing constraints between adjacent a-value bins is visible—these smooth the distributions along the x-axis.)

Average inversion results for $6 \le M < 7$, $7 \le M < 8$, and $M \ge 8$ mainshocks are shown in Figure 7a. We find that there is less intersequence variability among sequences with larger mainshock magnitudes. This could be because larger mainshocks are sampling local aftershock productivity within a larger volume, thereby averaging out some of the local variability. To make sure that the differences we observe are not due to the inversion, we perform a synthetic test where all mainshock magnitude bins have the same underlying variability. The results shown in Ⓔ Figure S5 show that, although the inversion does somewhat smear out the a-value distribution, it recovers the true mean and does not artificially generate the mainshock magnitude dependence that we see in Figure 7a.

The mean Omori a-values also show small differences between the mainshock magnitude bins; however, we suspect that this is not signal but noise, possibly due to systematic magnitude errors in the catalog, because the mean values do not change in a consistent way (the highest a-value is in the intermediate mainshock magnitude bin).

Stacked inversion results for all mainshock magnitudes are shown in Figure 7b. These are well-fit by a Gaussian distribution with a mean of $a = -2.54$ and a standard deviation of 0.71. The mean of the distribution is different from the a-value of the global stack shown in Figure 4 because the number of aftershocks scales as 10^a. Productive aftershock sequences dominate the stack, and the mean number of aftershocks observed per sequence is larger than the typical, median number of aftershocks observed.

Next, we invert for the intersequence a-value distribution in each of the 13 García *et al.* (2012) regions. Because of the paucity of data in some of the tectonic regions, in the regional

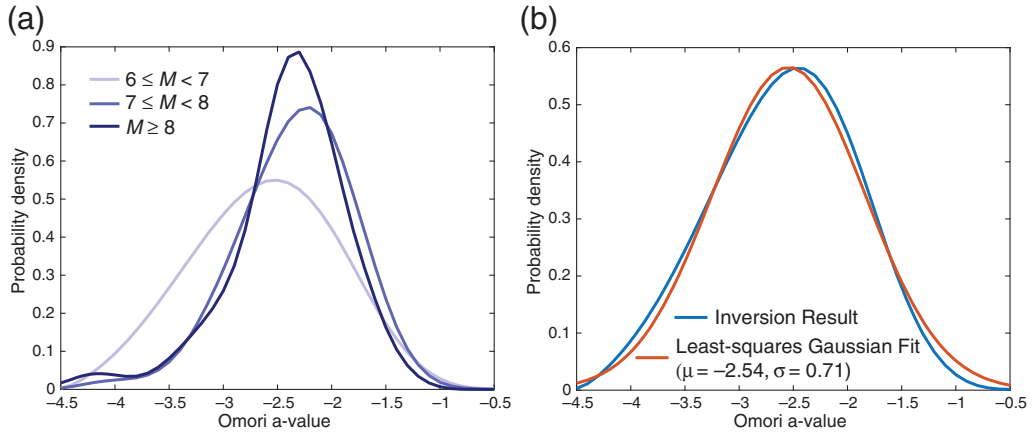

Figure 7. (a) Average inversion results for the distribution of Omori a-values among sequences in different mainshock magnitude intervals. (b) Average inversion results for all mainshock magnitudes, compared to the least-squares Gaussian fit.

fits we remove mainshock magnitude dependence (aside from the scaling of aftershock rate with mainshock magnitude assumed in equation 3) from the parameterization for the a-value distribution. Thus, our model vector $\mathbf{x}$ for the regional fits is a probability distribution for a. Inverted a-value distributions for each region, along with Gaussian fits, are shown in Figure 8.

We can use our global results to recover the mainshock magnitude dependence of the productivity variability in the regional fits. We assume that the variance in the Omori a-value consists of two terms:

$$\sigma^2 = \sigma_0^2 + \frac{\sigma_1^2}{10^{M_{\text{main}}}}. \tag{8}$$

The first term represents productivity variability due to mainshock magnitude error or gross source properties, apart from area. The second term is an additional variance that is reduced as mainshock area increases (because local aftershock productivity will be averaged over larger areas as mainshock area increases). We assume that σ_0 is constant and σ_1 is region-dependent. Because of the area dependence, this formulation predicts that regions with higher mean stress drop (and thus smaller rupture areas) will have increased intersequence aftershock productivity variability. This is indeed what we see in the regional inversion results; SCR-GENERIC, for example, has a much higher variability than ANSR-SHALCON or SZ-GENERIC, which is consistent with the high stress drops observed in stable continental regions (Allmann and Shearer, 2009).

From the global inversion results, we obtain a best fit to the distributions as a function of mainshock magnitude (Fig. 7a) with $\sigma_0 = 0.49$ and $\sigma_1 = 750$. When equation (8) is integrated over all mainshock magnitudes, this predicts $\sigma = 0.72$, which agrees closely with the stacked inversion result (Fig. 7b) of $\sigma = 0.71$.

Assuming $\sigma_0 = 0.49$ for the individual tectonic regions, we fit the regional inversion results (Fig. 8) to obtain σ_1 for each region. The results are given in Table 1. These values can be used to generate mainshock-magnitude-dependent distributions for the Omori a-value for each tectonic region.

Combining Generic- and Sequence-Specific Information

The region-specific p-values and a-value distributions presented in this article can be used to generate aftershock probability forecasts immediately following an earthquake. As time passes and aftershocks are recorded, these initial estimates can then be updated with sequence-specific information. Bayes' rule provides a formal way to do this updating; the regional a-value distribution can be used as a prior, and then updated using aftershock data. The posterior distribution for the a-value distribution is proportional to the product of the prior distribution and the data likelihood (equation 7).

An example of Bayesian updating as a sequence progresses is shown in Figure 9, which shows prior and posterior distributions for the Omori a-value at various times following the 2010 M_w 8.8 Maule, Chile, earthquake. The prior distribution uses the region-specific a-value distribution for the SZ-GENERIC region, modified using equation (8) to account for the mainshock magnitude. This prior distribution can be updated based on available aftershock data at various time intervals following the mainshock, which progressively shrinks the uncertainty in a.

Bayesian updating has the advantage of smoothly changing aftershock probabilities as more information is gathered about the sequence. The likelihood function will penalize a-values that are not consistent with the recorded data and allows for updating of the prior probability in situations where the rate is low or even in situations where no aftershocks have been recorded over a period of time. Reasenberg and Jones (1989) also advocate Bayesian updating; in their case, they present prior distributions that can be used to update a, p, and b simultaneously. Although Reasenberg and Jones (1989) parameters are currently used for USGS aftershock alerts in California, formal Bayesian updating is

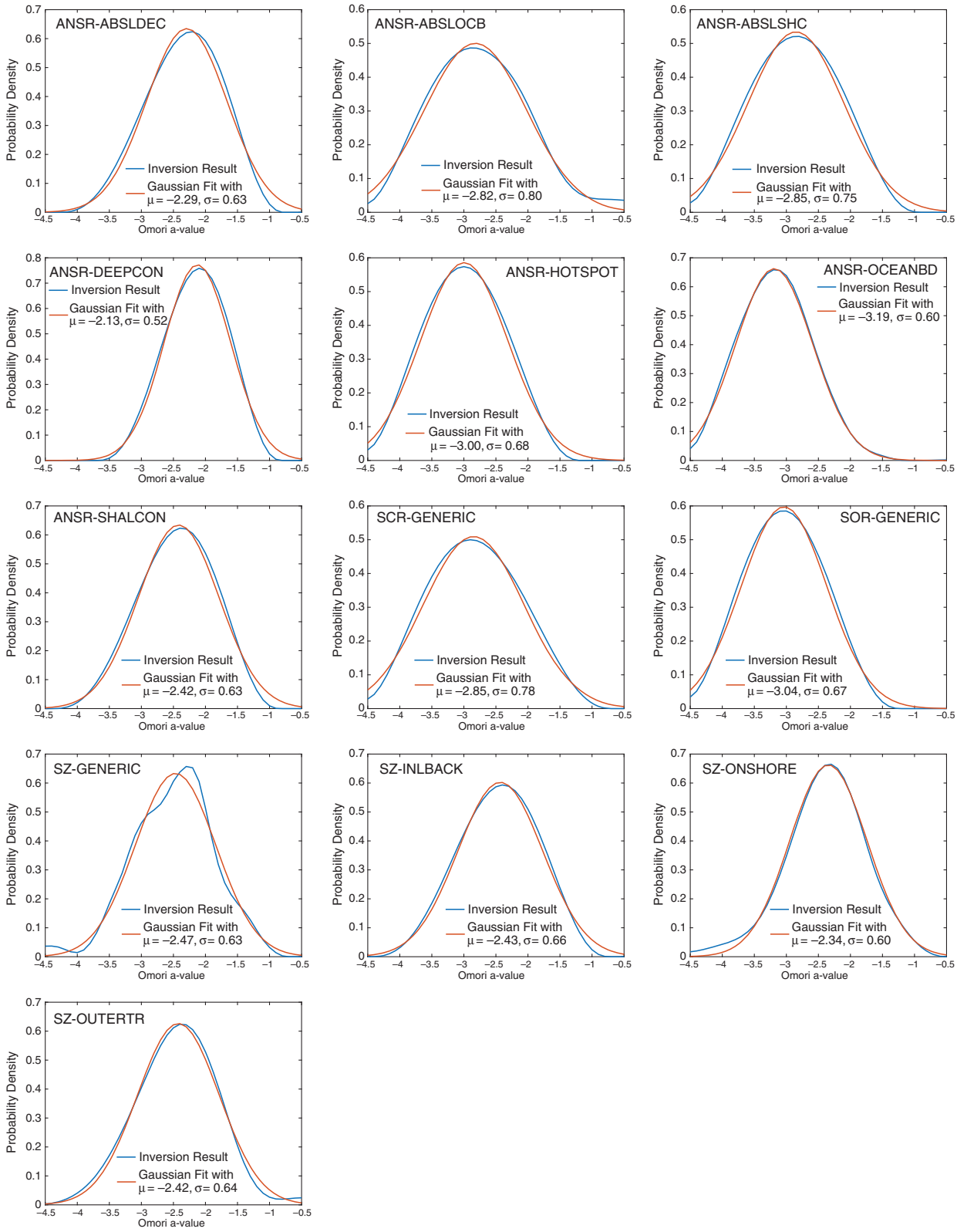

Figure 8. Inverted *a*-value distributions for García *et al.* (2012) tectonic regions and Gaussian fits to these distributions.

Table 1
Estimates of the σ_1 Component of Intersequence Aftershock Productivity Variability, Assuming Equation (8) and $\sigma_0 = 0.49$

Region	σ_1
ANSR-ABSLDEC	560
ANSR-ABSLOCB	890
ANSR-ABSLSHC	800
ANSR-DEEPCON	250
ANSR-HOTSPOT	680
ANSR-OCEANBD	500
ANSR-SHALCON	570
SCR-GENERIC	870
SOR-GENERIC	650
SZ-GENERIC	570
SZ-INLBACK	640
SZ-ONSHORE	500
SZ-OUTERTR	540

not used. Here, we show a method to update only the a-value, which is potentially more stable than simultaneously updating a, p, and b. One could attempt to update more than just the Omori a-value and keep the probability estimates stable using tight priors for the p-value or both p and b.

Discussion and Conclusions

One way to check the accuracy of our estimations, including our $\alpha = b$ assumption, is a comparison to Båth's law (Richter, 1958), the magnitude difference between a mainshock and its largest aftershock. Båth's law is a useful measure of productivity in that it is insensitive to catalog incompleteness; however, it does only use one aftershock from each sequence, so it uses less information than a whole sequence fit. We compare the median Båth's law value, because this can be calculated as long as at least half of the sequences have at least one aftershock.

Table 2 compares median Båth's law values for each region to the values implied by the mean Omori parameter fits (from the stack of all sequences) as well as the distribution of a-values found by the inversion method. Implied Båth's law values from the mean Omori parameters systematically underpredict the actual measured Båth's law values from the catalog. This is to be expected because the mean parameters are more productive than the median aftershock sequence. When we use the a-value distribution to account for intersequence variability, the actual and implied Båth's law values match quite well. In fact, the correlation between the shift in implied Båth's law values between the mean parameter predictions and a-value distribution predictions correlates positively with the difference between the implied Båth's law values for the mean parameters and the actual parameters from the catalog (linear correlation of 0.60)—which demonstrates that the differences in a-value distributions between regions are robust—they are as wide as they need to be in each region to bring the Båth's law values into alignment.

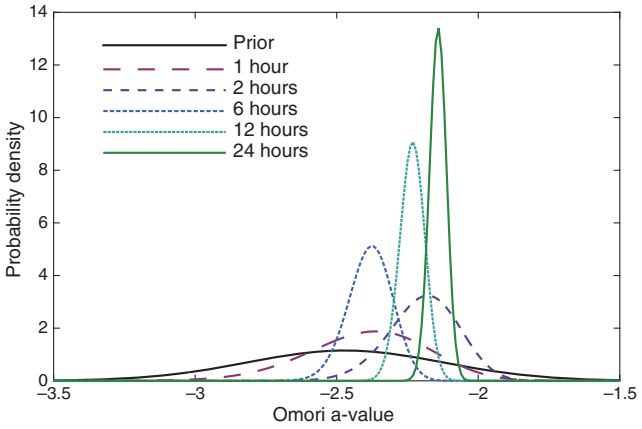

Figure 9. Posterior distribution example using the 2010 M_w 8.8 Maule, Chile, earthquake. Immediately following the earthquake, the region-specific Omori a-value distribution can be used. The distribution shown is for the SZ-GENERIC region, using mainshock magnitude dependence (Table 1). As the aftershock sequence progresses and additional data are collected, this distribution can be treated as a prior distribution and updated using Bayes' rule. Posterior distributions at subsequent time intervals are shown.

The reader may note that the measured Båth's law values in Table 2 are higher than the oft-quoted value of 1.2. These are 10-day Båth's law values (in contrast to many published values, which do not give a time interval, e.g., Richter, 1958; Båth, 1965), and they are median values. We do find a mean 10-day Båth's law value for global $M \geq 6.0$ mainshocks of 1.17 if the ~40% of sequences without a recorded aftershock above $M_{cat} = 4.5$ are excluded. For $M_{main} \geq 8.1$, there is at least one aftershock for all global sequences, allowing the mean Båth's law value to be defined; this leaves 16 sequences and gives a mean 10-day Båth's law value of 1.4.

Differences in productivity between regions vary by almost an order of magnitude. The most productive regions ANSR-ABSLDEC and SZ-OUTERTR are 5–9 times more productive in the first 10 days of sequences than the least productive regions SOR-GENERIC and ANSR-HOTSPOT. Even in regions where there are very little data, the data that are available show significant differences in productivity between regions.

The differences in intersequence productivity are more difficult to interpret. On the one hand, the inversion method we use requires some regularization because the inverse problem is underdetermined due to sequences without aftershocks. We choose to regularize via smoothing, which has the effect of smearing out the a-value distributions and making it difficult to recover the true intersequence variability. Although we use the same weight on the smoothing constraint for all regions, the smoothing constraint may have more relative power in regions with little data (i.e., in regions where the data power is low). However, our Båth's law values using these distributions agree well with the actual catalog—and on a region-by-region basis, our inverted a-value distributions recover the actual Båth's law values

Table 2
Comparison of Implied Median 10-Day Båth's Law Estimates from Parameter Fits to Measured Median Båth's Law Values from the Catalog

Region	Estimated Omori a-Value	Estimated Omori p-Value	Implied Båth's Law Value (Stack)*	Implied Båth's Law Value (Distribution)†	Actual Båth's Law Value (Catalog)	Number of Sequences (M_{main} Range)‡
ANSR-ABSLDEC	−2.04	1.01	1.11	1.32	1.25	40 ($M \geq 6.0$)
ANSR-ABSLOCB	−2.00	0.64	1.12	1.82	1.7	31 ($M \geq 6.3$)
ANSR-ABSLSHC	−2.44	1.06	1.47	1.81	1.9	9 ($M \geq 6.5$)
ANSR-DEEPCON	−2.01	0.98	1.09	1.17	1.35	86 ($M \geq 6.0$)
ANSR-HOTSPOT	−2.84	1.12	1.83	1.93	0.8§	3 ($M \geq 6.4$)
ANSR-OCEANBD	−2.69	1.08	1.71	2.13	2.05	74 ($M \geq 6.6$)
ANSR-SHALCON	−2.16	0.98	1.23	1.45	1.5	40 ($M \geq 6.0$)
SCR-GENERIC	−2.28	0.73	1.38	1.86	1.9	5 ($M \geq 6.4$)
SOR-GENERIC	−2.98	0.97	2.03	2.03	2.1	3 ($M \geq 6.6$)
SZ-GENERIC	−2.09	0.88	1.20	1.52	1.5	935 ($M \geq 6.0$)
SZ-INLBACK	−2.09	0.86	1.20	1.48	1.5	29 ($M \geq 6.0$)
SZ-ONSHORE	−2.02	0.81	1.13	1.42	1.5	225 ($M \geq 6.0$)
SZ-OUTERTR	−1.97	0.92	1.07	1.48	1.6	142 ($M \geq 6.1$)

*Median Båth's law values using the mean estimated Omori parameters from fit to stacked sequences (Fig. 5).
†Median Båth's law values using the mean estimated p-value and the a-value distribution (from inversion, Fig. 8).
‡Number of sequences used and minimum mainshock magnitude used for catalog-based Båth's law estimate. For each region, we choose the smallest cutoff in mainshock magnitude such that the median Båth's law value is defined for $M_{cat} = 4.5$.
§This is quite lower than the parameter-implied Båth's law values; however, eight sequences at $M \geq 6.0$ imply a median Båth's law value ≥ 1.5.

from the catalog far better than applying a single a-value uncertainty to each region would do.

Because of the significant differences in productivity between regions, and our good regional Båth's law fits using our a-value distributions, we conclude that the García *et al.* (2012) tectonic regions are useful for the purpose of generic aftershock parameter estimation. The regional fits are more informative than the global fits, and the additional information that the tectonic region provides is useful, particularly early in the sequence before significant aftershock data have been recorded. Better regionalization for the purposes of teasing out difference between aftershock parameters may certainly exist, and there is likely utility in fitting data in smaller regions where there are good regional networks. As the García *et al.* (2012) tectonic regions were developed for the purposes of regionalizing ground-motion prediction equations, their utility here is a pleasant surprise.

Data and Resources

The National Earthquake Information Center (NEIC) catalog, also known as ComCat, is available at http://earthquake.usgs.gov/earthquakes/search/ (last accessed September 2015). Because the ComCat catalog is not currently versioned, we provide the catalog we used in this analysis (https://github.com/mtpage/Aftershocks, last accessed April 2016). This link also contains MATLAB codes to sort the catalog into mainshock/aftershock sequences and reproduce the regional Omori fits shown in Figure 5. Code to apply the Flinn–Engdahl-based regionalization scheme is available at https://github.com/usgs/strec (last accessed April 2016).

Acknowledgments

We thank Mike Hearne for providing code and documentation for National Earthquake Information Center's (NEIC) current implementation of Flinn–Engdahl tectonic regionalization. In addition, we thank Kevin Milner for providing additional code and computational support to batch load large earthquake catalogs. We also thank Andrea Llenos and Peter Powers for internal reviews, and several anonymous reviewers for useful comments.

References

Aki, K. (1965). Maximum likelihood estimate of b in the formula $\log N = a - bM$ and its confidence limits, *Bull. Earthq. Res. Inst.* **43,** 237–239.

Allmann, B. P., and P. M. Shearer (2009). Global variations of stress drops for moderate to large earthquakes, *J. Geophys. Res.* **114,** no. B1, doi: 10.1029/2008JB005821.

Båth, M. (1965). Lateral inhomogeneities in the upper mantle, *Tectonophysics* **2,** 483–514.

Felzer, K. R., R. E. Abercrombie, and G. Ekström (2003). Secondary aftershocks and their importance for aftershock forecasting, *Bull. Seismol. Soc. Am.* **93,** 1433–1448, doi: 10.1785/0120020229.

Felzer, K. R., R. E. Abercrombie, and G. Ekström (2004). A common origin for aftershocks, foreshocks, and multiplets, *Bull. Seismol. Soc. Am.* **94,** 88–98, doi: 10.1785/0120030069.

Flinn, E. A., and E. R. Engdahl (1965). A proposed basis for geographical and seismic regionalization, *Rev. Geophys.* **3,** 123–149, doi: 10.1029/RG003i001p00123.

Frohlich, C., and S. D. Davis (1993). Teleseismic b values—Or, much ado about 1.0, *J. Geophys. Res.* **98,** 631–644, doi: 10.1029/92JB01891.

García, D., D. J. Wald, and M. G. Hearne (2012). A global earthquake discrimination scheme to optimize ground-motion prediction equation selection, *Bull. Seismol. Soc. Am.* **102,** 185–203, doi: 10.1785/0120110124.

Gutenberg, B., and C. F. Richter (1944). Frequency of earthquakes in California, *Bull. Seismol. Soc. Am.* **4,** 185–188.

Hainzl, S. (2016). Rate-dependent incompleteness of earthquake catalogs, *Seismol. Res. Lett.* **87,** 337–344, doi: 10.1785/0220150211.

Helmstetter, A., Y. Y. Kagan, and D. D. Jackson (2005). Importance of small earthquakes for stress transfers and earthquake triggering, *J. Geophys. Res.* **110,** no. B5, doi: 10.1029/2004JB003286.

Helmstetter, A., Y. Y. Kagan, and D. D. Jackson (2006). Comparison of short-term and time-independent earthquake forecast models for Southern California, *Bull. Seismol. Soc. Am.* **96,** 90–106.

Jordan, T., Y.-T. Chen, P. Gasparini, R. Madariaga, I. Main, W. Marzocchi, G. Papadopoulos, G. Sobolev, K. Yamaoka, and J. Zschau (2011). Operational earthquake forecasting: State of knowledge and guidelines for implementation, *Ann. Geophys.* **54,** 316–391.

Kagan, Y. Y. (2004). Short-term properties of earthquake catalogs and models of earthquake source, *Bull. Seismol. Soc. Am.* **94,** 1207–1228.

Lawson, C. L., and R. J. Hanson (1974). *Solving Least Squares Problems*, Prentice-Hall, Englewood Cliffs, New Jersey.

Llenos, A. L. (2014). The (un)productivity of the 2014 M 6.0 South Napa aftershock sequence, *AGU Fall Meeting*, Abstract Number S33F-4928.

Ogata, Y. (1988). Statistical models for earthquake occurrence and residual analysis for point processes, *J. Am. Stat. Assoc.* **83,** 9–27.

Ogata, Y., and K. Katsura (2006). Immediate and updated forecasting of aftershock hazard, *Geophys. Res. Lett.* **33,** no. 10, doi: 10.1029/2006GL025888.

Omi, T., Y. Ogata, Y. Hirata, and K. Aihara (2014). Estimating the ETAS model from an early aftershock sequence, *Geophys. Res. Lett.* **41,** no. 3, 850–857, doi: 10.1002/2013GL058958.

Omori, F. (1895). On after-shocks of earthquakes, *J. Coll. Sci. Imp. Univ. Tokyo* **7,** 111–200.

Reasenberg, P. A., and L. M. Jones (1989). Earthquake hazard after a mainshock in California, *Science* **243,** 1173–1176.

Richter, C. F. (1958). *Elementary Seismology*, W. F. Freeman, San Francisco, California.

Ringdal, F. (1975). Estimation of seismic detection thresholds, *Bull. Seismol. Soc. Am.* **65,** 1631–1642.

Shi, Y., and B. A. Bolt (1982). The standard error of the magnitude-frequency *b* value, *Bull. Seismol. Soc. Am.* **72,** 1677–1687.

Utsu, T. (1957). Magnitude of earthquakes and occurrence of their aftershocks, *Zisin2* **10,** no. 1, 35–45.

Utsu, T. (1972). Aftershocks and earthquake statistics (3): Analyses of the distribution of earthquakes in magnitude, time and space with special consideration to clustering characteristics of earthquake occurrence (1), *J. Facul. Sci., Hokkaido Univ. Ser. 7, Geophys.* **3,** 379–441.

Utsu, T., Y. Ogata, and R. S. Matsu'ura (1995). The centenary of the Omori formula for a decay law of aftershock activity, *J. Phys. Earth* **43,** 1–33.

Wells, D. L., and K. J. Coppersmith (1994). New empirical relationships among magnitude, rupture length, rupture width, rupture area, and surface displacement, *Bull. Seismol. Soc. Am.* **84,** 974–1002.

Wiemer, S., and M. Wyss (2000). Minimum magnitude of completeness in earthquake catalogs: Examples from Alaska, the western United States, and Japan, *Bull. Seismol. Soc. Am.* **90,** 859–869.

Young, J., B. Presgrave, H. Aichele, D. Wiens, and E. Flinn (1996). The Flinn–Engdahl regionalisation scheme: The 1995 revision, *Phys. Earth Planet. In.* **96,** 223–297, doi: 10.1016/0031-9201(96)03141-X.

U.S. Geological Survey
525 South Wilson Avenue
Pasadena, California 91106
pagem@caltech.edu
nvanderelst@usgs.gov
kfelzer@usgs.gov
(M.T.P., N.v., K.F.)

U.S. Geological Survey
345 Middlefield Road
Menlo Park, California 94025
jhardebeck@usgs.gov
michael@usgs.gov
(J.H., A.J.M.)

Manuscript received 4 March 2016;
Published Online 23 August 2016